J Mater Sci (2012) 47:815–823
DOI 10.1007/s10853-011-5859-z

Studying grain boundary regions in polycrystalline materials using spherical nano-indentation and orientation imaging microscopy

Siddhartha Pathak · Johann Michler · Kilian Wasmer · Surya R. Kalidindi

Received: 24 June 2011 / Accepted: 6 August 2011 / Published online: 18 August 2011

Abstract In this article, we report on the application of our spherical nanoindentation data analysis protocols to study the mechanical response of grain boundary regions in as-cast and 30% deformed polycrystalline Fe–3%Si steel. In particular, we demonstrate that it is possible to investigate the role of grain boundaries in the mechanical deformation of polycrystalline samples by systematically studying the changes in the indentation stress–strain curves as a function of the distance from the grain boundary. Such datasets, when combined with the local crystal lattice orientation information obtained using orientation imaging microscopy, open new avenues for characterizing the mechanical behavior of grain boundaries based on their misorientation angle, dislocation density content near the boundary, and their propensity for dislocation source/sink behavior.

S. Pathak · J. Michler · K. Wasmer
EMPA, Swiss Federal Laboratory for Materials Science and Technology, Feuerwerkerstrasse 39, 3602 Thun, Switzerland

S. Pathak (✉) · S. R. Kalidindi
Department of Materials Science and Engineering, Drexel University, Philadelphia, PA 19104, USA
e-mail: pathak@caltech.edu; siddharthapathak@gmail.com

Present Address:
S. Pathak
Materials Science, California Institute of Technology (Caltech), 1200 E. California Blvd., MC 309-81, Pasadena, CA 91125-8100, USA

S. R. Kalidindi
Department of Mechanical Engineering and Mechanics, Drexel University, Philadelphia, PA 19104, USA

Introduction

Grain boundaries play an important role in the mechanical response of polycrystalline metals. The well-known Hall–Petch effect [1, 2] relates the increase in yield strength to a decrease in the average grain size in the sample through a power-law expression. Although the effect is clearly established, its physical origins are a matter of debate in literature [3, 4]. The physical explanations for the Hall–Petch effect generally assume either dislocation pile-ups [1, 2] or higher dislocation densities in the grain boundary regions [5]. The dislocation pile-up model implicitly assumes that the grain boundaries are not effective as dislocation sinks. On the other hand, the models that invoke higher dislocation densities in the grain boundary regions (compared to the bulk of the grain) rely on grain boundaries serving as effective sources of dislocations [6]. In this article, we outline a new methodology for studying these effects across individual grain boundaries using spherical nanoindentation stress–strain curves.

Mechanical studies involving grain boundaries have traditionally been conducted on macroscopic specimens containing multi-grained microstructures, and only recently researchers have started to interrogate the mechanical response of materials at the scale of individual grain boundaries. Among the experimental techniques available at these length scales, nanoindentation, with its high resolution load and depth sensing capabilities, shows the greatest promise due to its ease of experimentation and versatility [7, 8]. In particular, using spherical indenters, our recent work [9–11] has demonstrated the feasibility of transforming the raw load–displacement data into meaningful indentation stress–strain curves. These indentation data analyses methods have captured successfully the local loading and unloading elastic moduli, the local indentation

yield strengths, and certain aspects of post-yield strain hardening behavior in various polycrystalline metal samples. More specifically, the use of these indentation stress–strain curves makes it possible to analyze the initial loading segments of spherical indentation; before the indentation itself imposes additional local plastic deformation and alters the local microstructure and its properties. This has enabled the measurement of the local indentation yield strengths in individual grains of deformed polycrystalline metallic samples, which in turn can be related to percentage increases in the local slip resistances from their fully annealed conditions [12]. In this paper, we apply these methods to indentations across grain boundaries showing their potential in investigating the role of grain boundaries in the mechanical response of polycrystalline samples.

Other than nanoindentation certain other techniques of testing miniaturized samples, such as compression testing of micro-pillars containing grain boundaries produced by removing material around a selected region of interest using a focused-ion beam (FIB), have also shown promise in examining the mechanical behavior of grain boundaries [13]. However, these techniques typically require tremendous resources in terms of sample preparation, test conditions and operator time, which make their large scale use uneconomical.

Prior attempts to study the mechanical response of grain boundary regions using indentation have been mostly limited to measuring the hardness and modulus using sharp (Vickers, Berkovich, cube corner) indenters. However, most studies have found hardness to be a poor indicator for measuring grain boundary strengthening effects [14, 15]. Only one study [16] has reported a significant change of hardness close to grain boundary, but these results could not be reproduced by others [17]. It is interesting to note that the few studies which have reported a weak dependence of hardness on the distance from the grain boundary have all used very low maximum loads for their hardness measurements [18–23]. This was studied systematically in the work of Eliash et al. [24] who noted that the width of their grain boundary-affected zone in molybdenum decreased with increasing maximum indentation loads, and for indentation loads exceeding 10 mN (using a Berkovich indenter), the trend vanishes. These studies point to the importance of calculating the contact stresses at or close to yield in indentation experiments.

The focus of the above mentioned studies has been primarily on measuring the resistance offered by grain boundaries to dislocation transmission across them. In these studies, the sharp indenters introduced substantial amount of plastic deformation in the sample before the dislocations were pushed to the grain boundaries and impeded by them. Therefore, the plastic deformation introduced by indentation in those experiments is likely to influence strongly the mechanical property being measured. The approach taken in this study is fundamentally different. The use of spherical indentation and our indentation data analyses protocols allow us to estimate the local indentation yield strength from the initial loading segment. In this way, the characterized property (the initial indentation yield point from the loading segment) corresponds to the intact material at the indentation site, and can be used to differentiate between inherent differences in the local material structure at the indentation site. Using Orientation Imaging Microscopy (OIM) [25, 26], which is based on automated indexing of back-scattered electron diffraction patterns, the structure information at the indentation site is then correlated with the mechanical data obtained from nanoindentation. In particular, in this study we demonstrate the capability of our techniques to measure the differences in indentation modulus and yield stresses across grain boundaries both as a function of the grain boundary character (high versus low angle grain boundary measured using OIM), and imposed cold work on the sample.

In addition, our investigations also revealed a new method for characterizing the dislocation source/sink behavior of grain boundaries by monitoring the (lack of) pop-ins in the vicinity of some (but not all) grain boundaries. The pop-in or strain burst being referred to here is the first pop-in in the sample under the indenter at lower loads [27], and should not be confused with the grain boundary induced pop-ins that occurs at much higher indentation loads and depths (hundreds of nanometers) [15, 22, 28]. As discussed in this article, the decrease in the propensity of pop-ins in the near-grain boundary regions in annealed samples could be used to quantify their potency as effective dislocation sources.

Materials and methods

Polycrystalline as-cast samples of Fe–3%Si steel, sectioned from the chill zone of a directionally solidified electrical steel ingot, were used in this study. We selected these particular samples since we have already established a number of the experimental protocols and the orientation dependence of indentation yield strength in annealed crystals in this material [12, 27]. These samples exhibited extremely large grains (of the order of few millimeters in effective grain size). One sample was given a 30% reduction in simple compression at room temperature to produce a moderately deformed microstructure.

Surface preparation is known to influence the extraction of indentation stress–strain curves from spherical nanoindentation on metal samples, as discussed in detail in our earlier report [27]. Following the procedure outlined in [27], the samples (as-cast as well as 30% deformed) were

prepared for indentation using a Buehler grinding and polishing machine. After grinding with SiC papers, 3 and 1 μm diamond suspensions were used for polishing the samples in conjunction with several intermediate etches by Nital (5% volume mixture of nitric acid in ethanol). The samples were subsequently polished using 0.05 μm colloidal silica. Two approaches were followed for removing the disturbed surface layer caused by mechanical polishing. For one set of both the as-cast and 30% deformed samples, the final step included vibratory polishing with 0.02 μm colloidal silica on a Buehler vibratory polisher for several (2–4) days. Another sample set was electropolished at room temperature using a mixture of 95% acetic acid and 5% perchloric acid at a voltage of 60–90 V and a current of 0.5–1 A.

OIM scans on the samples (as-cast as well as deformed) were already obtained in a previous study [12]. Based on the OIM scans, three grains in the as-cast sample (labelled 1, 2, and 3) and two grains in the 30% deformed sample (labelled 4 and 5) were chosen for this study. In particular, the boundaries between Grains 1 and 2 (high mis-orientation angle in annealed condition), 2 and 3 (low mis-orientation angle in annealed condition), and 4 and 5 (high mis-orientation angle in the deformed condition) were studied by nanoindentation. The processing history of these samples (as described before) is such that the boundaries of the large (millimetre–range) grains studied here are expected to be nominally perpendicular to the sample surface. This was also verified by cutting ~10 μm deep trenches across the boundaries using FIB sections.

Nanoindentations were carried out using two different nanoindenters—the MTS XP® system maintained and operated by the Centralized Research Facilities in the College of Engineering at Drexel University, Philadelphia, USA, and the Agilent G200® system located at the Paul Scherrer Institut (PSI), Villigen, Switzerland. Both systems were equipped with the continuous stiffness measurement (CSM) attachment. Three different spherical diamond tips with radii of 1, 10, and 13.5 μm, respectively, were used in this study. The different radii of the indenters allow us to explore the influence of indentation length scales on the measurements. The indentations were performed on a line inclined at a shallow angle to the grain boundary, so as to allow more indents close to the grain boundary. The large grain sizes in our samples allowed us to perform between three to five lines of indents, with each line containing 20 indents spaced 10 μm apart, across each grain boundary for each indenter size. This resulted in at least 100 indents across every grain boundary. The rather larger number of indentations used in this study allows us to ensure that the mechanical trends across the grain boundaries can be clearly distinguished from the inherent experimental scatter present in nanoindentation measurements. The perpendicular distance from the center of the indent to the grain boundary line was calculated as the distance of the respective indent from the boundary. The indentation contact radius at maximum load for the smaller 1 μm indenter was around 400 nm for the samples studied here; for the larger 10 and 13.5 μm indenters, the indentation contact radius was around 1 μm. So the 10 μm spacing between indents should be sufficient to prevent any interference between neighboring indents.

The measured load–displacement data in spherical nanoindentation was converted into indentation stress–strain curves to allow a better analysis of the local mechanical response. The data analysis protocols are detailed in Ref. [9] and can be briefly summarized as a two-step procedure. The first step in the analysis process is an accurate estimation of the point of effective initial contact in the given data set, i.e., a clear identification of a zero-point that makes the measurements in the initial elastic loading segment consistent with the predictions of Hertz's theory [29–31]. As shown in Ref. [9], the zero point can be conveniently determined using the following equation for the initial elastic segment in a frictionless, spherical indentation:

$$S = \frac{3P}{2h_e} = \frac{3\left(\tilde{P} - P*\right)}{2\left(\tilde{h}_e - h*\right)} \tag{1}$$

where $\tilde{P}$, $\tilde{h_e}$, and S are the measured load signal, the measured displacement signal, and the continuous stiffness measurement (CSM) signal in the initial elastic loading segment from the machine, respectively, and $P*$ and $h*$ denote the values of the load and displacement values at the point of effective initial contact. Rearrangement of Eq. 1 reveals that a plot of $\tilde{P} - \frac{2}{3}S\tilde{h}_e$ against S will produce a linear relationship whose slope is equal to $-\frac{2}{3}h*$and the y-intercept is equal to P^*. A linear regression analysis can then be performed to identify the point of the effective initial contact (P^* and h^*) very accurately.

In the second step, the values of indentation stress and strain can be calculated by recasting Hertz theory for frictionless, elastic, spherical indentation as

$$\sigma_{\text{ind}} = E_{\text{eff}}\varepsilon_{\text{ind}},\ \sigma_{\text{ind}} = \frac{P}{\pi a^2},\ \varepsilon_{\text{ind}} = \frac{4}{3\pi}\frac{h_e}{a} \approx \frac{h_e}{2.4a},$$
$$a = \frac{S}{2E_{\text{eff}}},\ \frac{1}{E_{\text{eff}}} = \frac{1-\nu_s^2}{E_s} + \frac{1-\nu_i^2}{E_i},\ \frac{1}{R_{\text{eff}}} = \frac{1}{R_i} + \frac{1}{R_s}, \tag{2}$$

where σ_{ind} and ε_{ind} are the indentation stress and indentation strain, a is the radius of the contact boundary at the indentation load P, h_e is the elastic indentation depth, S (=dP/dh_e) is the elastic stiffness described earlier, R_{eff} and E_{eff} are the effective radius and the effective stiffness of the indenter and the specimen system, ν and E are the

Poisson's ratio and the Young's modulus, and the subscripts s and i refer to the specimen and the indenter, respectively.

Results and discussion

Effects of surface preparation and indenter size on pop-ins

Pop-ins or displacement bursts are a common feature in indentation measurements on samples with low dislocation densities. These are attributed to the fact that the indentation zone size in these experiments at the point of initiation of plastic strain under the indenter is comparable or smaller than the dislocation-network length scales in the sample (e.g., spacing of dislocations, dislocation cell size). The occurrence of the pop-ins can therefore be correlated to the difficulty of activating a dislocation source in the primary indentation zone. As expected, the propensity for pop-ins decreases with an increase in the indentation zone size (larger indenter radius), as well as with an increase in the dislocation density of the sample (e.g., in a deformed material) [27].

It is well-known that metal samples typically have a 5–10 nm-thick native oxide layer on their surfaces, and the breakup of such an oxide film could also result in pop-in events. However, no such pop-in events were found to occur in the 30% deformed Fe–3%Si samples (shown later in Fig. 4). Since the oxide layer thickness is expected to be identical in both samples (as-cast and deformed), the pop-ins seen in this study are not thought be due to the oxide layer breakup. This issue has been discussed in significant detail in our previous publication [27] as well.

Pop-ins, which appear as displacement bursts in a load versus displacement plot, manifest as strain bursts in indentation stress–strain curves. As seen in Fig. 1, an indentation stress–strain plot with an initial pop-in often exhibits a large discontinuity. This makes it difficult to accurately estimate the indentation yield strength (Y_{ind}) from such a plot. As-cast samples prepared using electropolishing are highly susceptible to this problem, as shown in Fig. 1a. In this study, we have vibro-polished one set of the as-cast samples with the hope of avoiding the pop-ins without significantly affecting the indentation yield strength. Representative indentation load–displacement curves and stress–strain curves obtained from the same grain in the as-cast sample with an electro-polished surface and a vibro-polished surface are compared to each other in Fig. 1a. The excellent agreement between the back-extrapolated Y_{ind} obtained on the electro-polished surface (with the pop-in) and the Y_{ind} measured on the vibro-polished surface (without

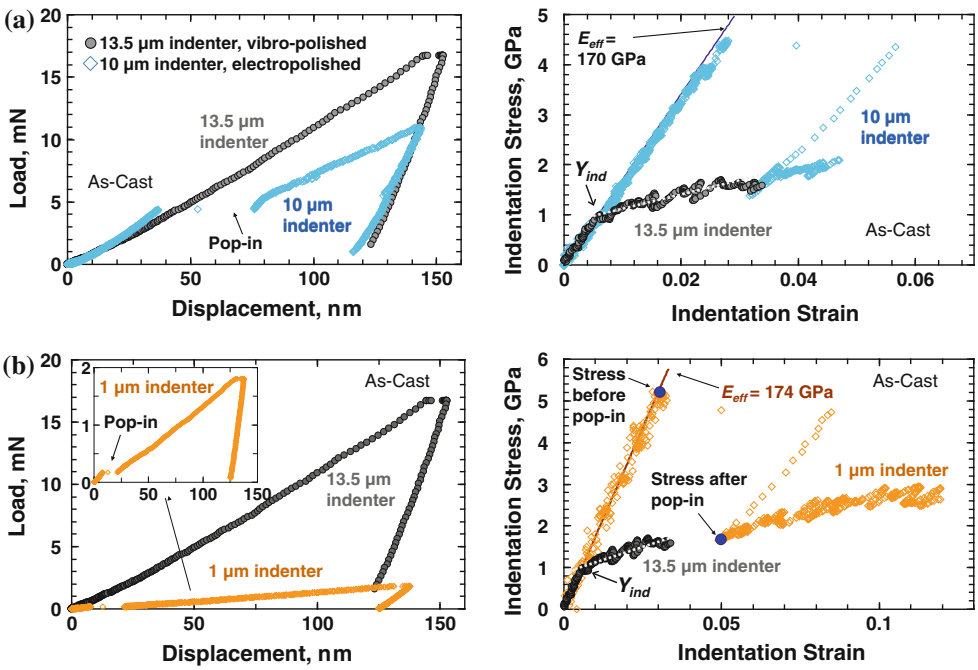

Fig. 1 **a** Effect of final surface finish: vibro-polish versus electro-polish. Indentations on the as-cast Fe–3%Si steel's electro-polished surface almost always result in a large pop-in. Pop-ins are usually suppressed on the vibro-polished surfaces when using the large 13.5 μm indenter. **b** Effect of indenter size: indents with the small 1 μm indenter show consistent pop-ins on the vibro-polished surface. The good agreements between the indentation stress–strain curves from different surface finishes and different indenter radii provide additional validation of the data analysis protocols used. The ratio of the stress before and after pop-in is used as an indicator of the ease of establishing a dislocation source in the indentation zone

the pop-in) was confirmed in numerous measurements on the sample. These measurements indicate that the vibro-polishing method introduces only a small number of dislocations into the sample surface, which are enough to suppress the pop-ins for the larger indenter sizes (10 and 13.5 μm radii) but do not appear to influence the measured Y_{ind} on the as-cast samples.

Figure 1b provides a comparison of the indentation stress–strain curves obtained in the same grain using the 1 and 13.5 μm indenters, both on vibro-polished surfaces. It is seen that the 1 μm indenter produces a large pop-in confirming that the amount of dislocations introduced during vibro-polishing is not large enough to suppress pop-ins at the small (1 μm radius) indenter sizes. The good agreement between the back-extrapolated Y_{ind} from the indentation stress–strain curve with the pop-in and the Y_{ind} from the indentation stress–strain curve without the pop-in, despite the big difference in the indenter radii, is quite reassuring. All of these observations indicate that it is viable to extract a value of the Y_{ind} on the vibro-polished surfaces of the as-cast samples.

Following the observations above, vibro-polishing was chosen as the final sample surface preparation step for the as-cast samples studied here. Vibro-polishing also reduces the possibility of developing a significant groove at the grain boundary that often results from electropolishing [19, 24]. Thus, for the present sample set, the smaller 1 μm radius indenter is ideal for studying the pop-in behavior in the grain boundary regions, while the larger 10 and 13.5 μm radii indenters, which seldom exhibit pop-ins, are ideally suited for estimating the Y_{ind} values in the same regions. The 30% deformed Fe–3%Si sample has a significantly larger dislocation density and hence no pop-ins are observed on this material irrespective of the indenter radius size and/or surface finish technique used [27].

Grain boundaries as dislocation sources

In order to examine the potential role of grain boundaries as dislocation sources, we examined the ratio of indentation stresses before and after the pop-in as a function of the distance from the grain boundary. As an example, the indentation stresses before and after pop-in on the indentation stress–strain curve are identified in Fig. 1b. It is suggested here that the ratio of these stresses can be used as a measure of the difficulty of establishing a dislocation source in the sample. In the limiting case where the pop-in disappears completely, this ratio becomes one and suggests that there was no difficulty in establishing a dislocation source.

As mentioned earlier, the pop-in behavior across grain boundaries was studied using the smaller 1 μm radius spherical indenter. In order to allow for more measurements, the indentations were performed on a line inclined at a shallow angle to the grain boundary as shown in Fig. 2. This approach allowed us to get many more measurements at varying distances from the grain boundary while ensuring that the indentations were sufficiently spaced to avoid any interference from each other.

Figure 2 shows two representative measurements on two different grain boundaries with two substantially different

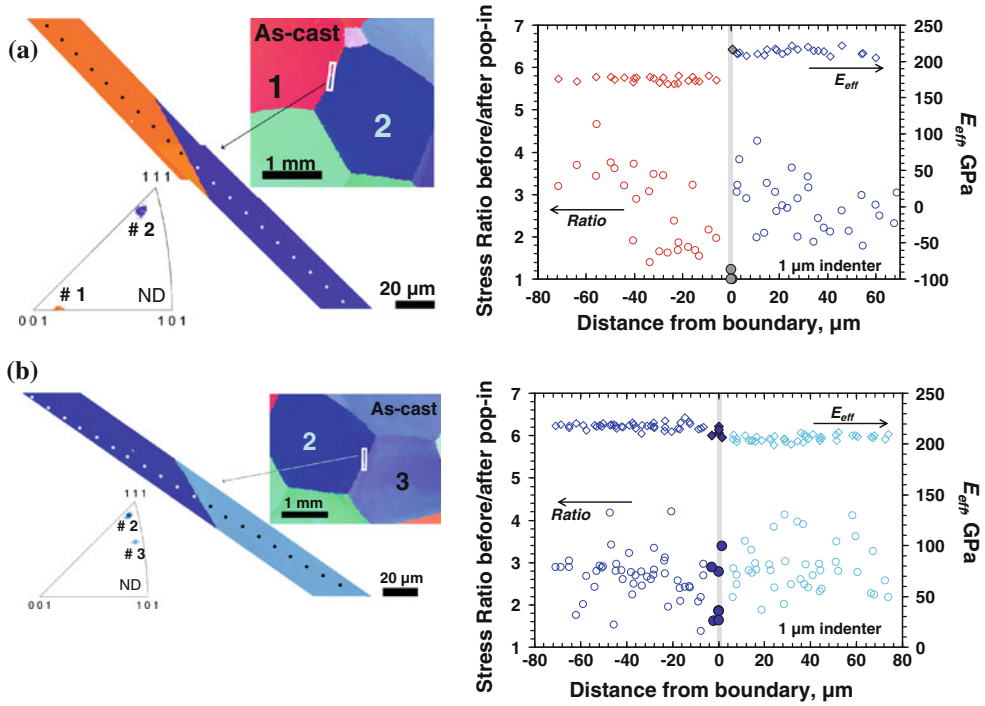

Fig. 2 Effective modulus (E_{eff}) and ratio of stresses before and after pop-ins across **a** a high angle grain boundary between Grains 1 and 2 and **b** a low angle grain boundary between Grains 2 and 3 in vibro-polished as-cast Fe–3%Si steel. The OIM maps show the location of a representative row of indents with respect to the corresponding boundaries

lattice misorientation angles. The OIM scans in Fig. 2 are color-coded to reflect the positions of the orientations in the inverse pole figure map using the standard convention (i.e., grains colored red, green, and blue have (001), (101), and (111) crystallographic planes parallel to the sample surface, respectively). In the indentation stress-ratio plots shown in Fig. 2, the grain boundary has been marked as a vertical line with a finite thickness. The thickness of this line reflects the region in which the primary indentation zone size at Y_{ind} includes the grain boundary. In other words, any indentation performed within the thickness of the vertical line shown as the grain boundary is expected to apply substantial stress on the grain boundary. The thickness of the line representing the grain boundary is calculated as $3a_{Y_{ind}}$, where $a_{Y_{ind}}$ is the contact radius at the indentation yield stress (following Ref. [9]).

Figure 2 shows the variance of the ratio of the indentation stress before and after pop-in with the distance from the grain boundary for the two boundaries depicted in the figure. It is seen that the grain boundary between Grains 1 and 2 is quite effective as a dislocation source (Fig. 2a), because the pop-ins essentially disappear in the indentations conducted at the grain boundary (reflected by the observation that the ratio of indentation stress before and after the pop-in goes to one). Note also the higher effective modulus (E_{eff}) for the near-(111) oriented Grain 2 as compared to the near-(001) oriented Grain 1 in Fig. 2a, denoting the high mismatch in stiffness between the two grains. Figure 2b also indicates that the other (low angle) grain boundary between Grains 2 and 3 is not as effective in suppressing the pop-ins, because the indentation stress ratio at the grain boundary has not changed significantly from the bulk of the grains. It is therefore clear from Fig. 2 that different grain boundaries exhibit different levels of potency in serving as dislocation sources in the deformation of polycrystalline materials, and the experimental protocols suggested here are capable of quantifying their effectiveness. Similar decrease and/or disappearance of the nanoindentation pop-ins in the vicinity of some (but not all) grain boundaries have been noted by other researchers as well [14, 19, 21, 22, 24, 28]. Obviously, it is important to repeat these measurements on a much larger number of grain boundaries to quantify the misorientation dependence of the grain boundary potency in serving as dislocation sources.

Grain boundaries regions in as-cast samples

As noted earlier, pop-ins can be suppressed using a larger indenter (see Figs. 1b, 3b). Therefore, we studied the changes in indentation moduli and yield strengths in the grain boundary regions in the as-cast samples using a larger 13.5 μm radius spherical indenter using the protocols

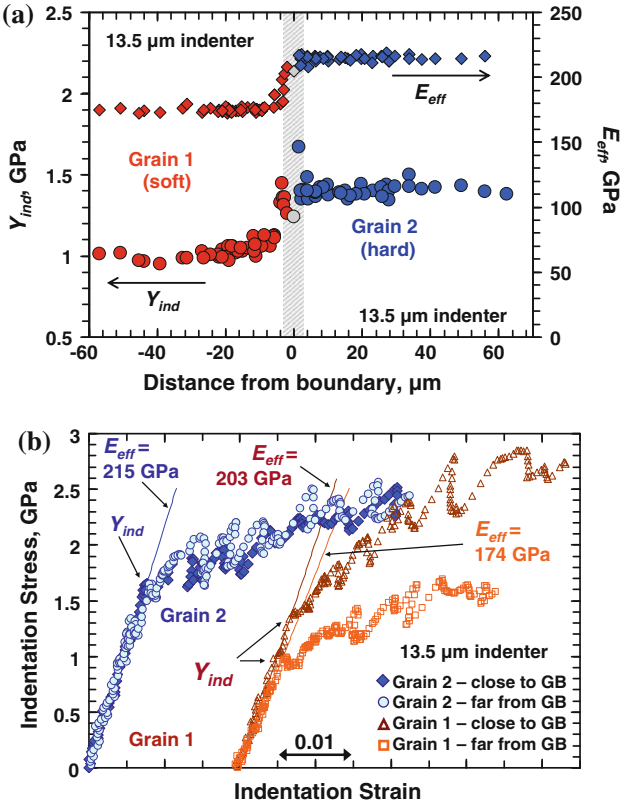

Fig. 3 **a** Measure of E_{eff} and Y_{ind} across the same high angle grain boundary shown in Fig. 2a. **b** Representative indentation stress–strain curves from the two grains showing the differences in mechanical responses between near grain boundary regions versus grain interiors

described earlier. The effective indentation modulus (E_{eff}) and the indentation yield strength (Y_{ind}) extracted from these measurements on the boundary between Grains 1 and 2 are plotted in Fig. 3a as a function of the distance from the grain boundary. The grains are labeled as 'soft' and 'hard' in a relative sense based on their indentation yield strengths. Note that the same grain boundary region in Fig. 3a is marked as a much wider region compared to Fig. 2 because of the larger indenter tip size in Fig. 3. Figure 3b shows representative indentation stress–strain curves in each grain for regions close to the grain boundary (that is indents placed within the thickness of the vertical line shown as the grain boundary in Fig. 3a), and far from the grain boundary.

Figure 3a provides strong validation for our protocols. The as-cast samples are not expected to have any excess dislocation storage at the grain boundaries. Therefore, both E_{eff} and Y_{ind} are fairly uniform in each grain and there is almost a step transition at the grain boundary. As expected, the indentation stress–strain curves in the regions adjacent to the grain boundary on the side of the soft grain show a composite effect with increases in both the indentation

modulus and the indentation yield strength reflecting contributions from both grains (see Fig. 3b).

Grain boundaries regions in deformed samples

Next, we studied selected grain boundary regions in the 30% compressed samples using the same protocols. As reported in our previous studies [12, 27], pop-ins do not appear in deformed samples where it is relatively easy to set up a dislocation source using the existing network of forest dislocations in the sample. Therefore, we investigated the grain boundary regions in the deformed samples using both small and large indenters, as well as both vibro-polished and electro-polished surfaces. A representative set of results from this study are presented in Fig. 4. Figure 4b shows representative indentation stress strain curves in each grain for regions close to and far from the grain boundary, while the summary of the E_{eff} and Y_{ind} values are shown in Fig. 4c.

As in the as-cast sample, the values of E_{eff} were fairly uniform in each grain of the 30% deformed sample as well and show a step like transition at the grain boundary. However, the variation of Y_{ind} indicated a substantial transition zone on one side of the grain boundary. The measurements are also remarkably consistent from all three indenters used in the study, despite the large range in the indenter tip radii. This level of consistency in the measurements provides additional validation for the protocols used in this study. No effects of the final surface polishing step (vibro-polish versus electro-polish) were observed.

In order to better understand the measurements of Y_{ind} shown in Fig. 4c, we have computed the percentage increases in the yield strength from the as-cast condition as a function of the distance from the grain boundary, as shown in Fig. 4d. As demonstrated in our recent study [12], it is possible to experimentally map the orientation dependence of the indentation yield strength for a given sample and to use this map for normalizing the indentation yield strength. This form of normalization accounts for the orientation dependence of the indentation measurements, and thus the percentage increase in the Y_{ind} can be interpreted as the percentage increase in the local slip resistance at the indentation site. This in turn can be interpreted as an indicator of the local dislocation density at the indentation site.

The Taylor factors in simple compression for Grains 4 and 5 were estimated using standard crystal plasticity models [32] to be 2.01 and 3.15, respectively. This suggests that Grain 5 should show more hardening as a result of the 30% compression compared to Grain 4. The measurements shown in Fig. 4d away from the grain boundary are in complete accord with this expectation.

However, it is seen from Fig. 4d that the grain boundary region on the side of Grain 5 accumulated much less dislocation density in the immediate vicinity of the grain boundary than far away from the boundary. Furthermore, it is seen that the dislocation density very near the grain boundary on the side of Grain 5 is also somewhat lower

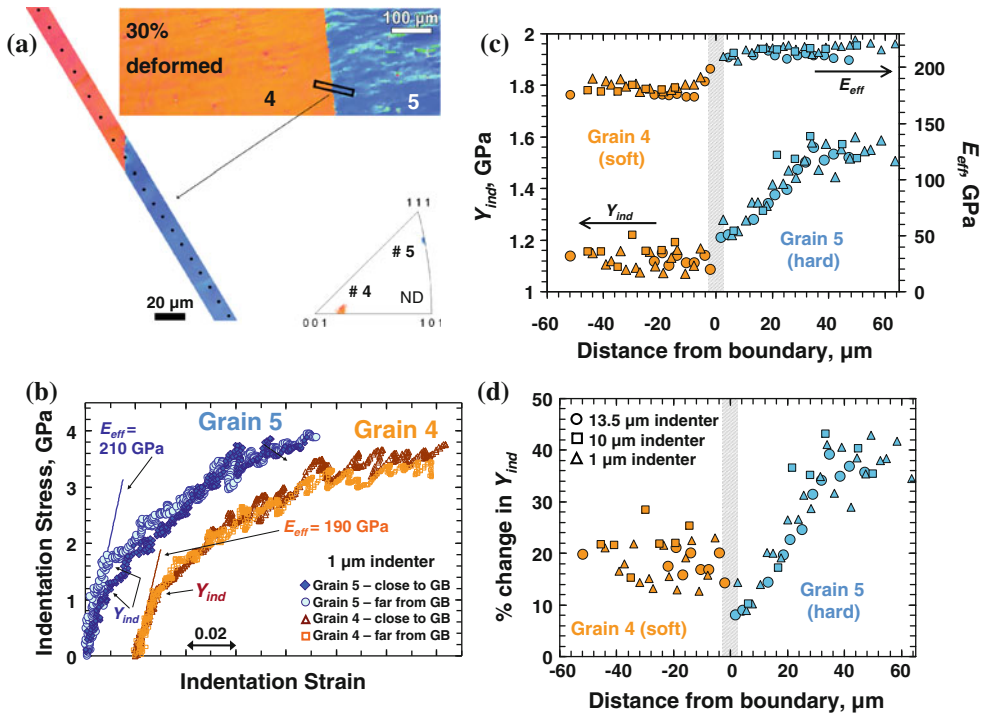

Fig. 4 **a** OIM maps of the 30% deformed Fe–3%Si steel sample showing the location of the indents with respect to the grain boundary. **b** Representative indentation stress–strain curves from the two grains showing the differences in mechanical responses between near grain boundary regions versus grain interiors. **c** Measure of E_{eff} and Y_{ind} across the grain boundary between Grains 4 and 5. **d** Estimate of the percentage change in Y_{ind} from the annealed condition following Ref. [12]

than the dislocation density in the grain boundary region on the side of Grain 4. These observations suggest that the nature of the grain boundary or the grain boundary character on both sides of a grain boundary can be substantially different from each other. In the example shown in Fig. 4, it is seen that the grain boundary on the side of Grain 5 acts as an efficient dislocation sink by absorbing the dislocations from the grain boundary region on the side of Grain 5.

We note here again that these samples were sectioned from a directionally solidified electrical steel ingot, and as such the grain boundaries explored in this study are expected be nominally vertical to the indentation surface. This was also verified by ~ 10 μm deep FIB cuts across the boundaries. Thus, any possibility of an inclined geometry of the boundaries below the surface is very remote. It is also noteworthy that these observations are consistent with previously reported observations in aluminum bicrystals based on high resolution measurements of orientation gradients on the sample surface [33–35].

Hardness across grain boundaries

It is emphasized here that insights obtained about the grain boundary regions from Figs. 3 and 4 are largely made possible by the use of our spherical nanoindentation data analyses protocols. In particular, computing the local indentation yield stress from the initial loading segment allows us to estimate the changes in the dislocation content at the indentation site, before the additional plastic strain induced by the indentation itself. This is in contrast to traditional hardness measurements using nanoindentation, where the contact stress at a specified load is typically measured after the material has experienced significant plastic strain. As a result, the conventional hardness measurements in the grain boundary regions fail to reveal meaningful trends. This is demonstrated in Fig. 5, where the variation of the local hardness is plotted as a function of the distance from the grain boundary. The hardness values in this case was estimated as the contact stress at 14 mN of load using the 13.5 μm indenter for the same grain boundary regions that are shown in Figs. 3 and 4. The hardness data shown in Fig. 5 does not reveal any discernable or useful trends. This observation was also reported by other researchers who have used indentation hardness to measure the mechanical response of grain boundaries [14, 15, 24]. The above discussion suggests that the initial indentation yield stress calculated from the loading segments of spherical indentation is a more reliable measure of the changes in the local dislocation density in the sample, and can potentially provide valuable new insights into the mechanical response of grain boundary regions.

Effect of indenter size

As noted earlier, indenter size strongly influenced the occurrence of pop-ins in the as-cast grains. In the experiments on deformed grains where there were no pop-ins, it was observed that the indenter size also strongly influenced the strain hardening rates observed in the indentation stress–strain curves. As an example, the indentation stress–strain curves obtained in the deformed Grain 5 using two different indenter sizes (1 and 10 μm radii) are shown in Fig. 6a. Although there is excellent agreement in the values of the indentation yield strength in the two indentation stress–strain curves, the post yield behaviors are substantially different.

In order to understand the differences in the post-yield behaviors for the different indenter sizes, we present in Fig. 6b the evolution of the contact radius corresponding to the two indentation stress–strain curves in Fig. 6a. It is seen that the contact radius for the smaller indenter is only about 100 nm at indentation yield. The indentation zone size can be estimated to be of the order of 2–3 times the contact radius [9]. In general dislocation cells sizes in most metals are reported to be of the order of 1 μm. Therefore, the length scale of the indentation zone for the small indenter may not be adequate to set up the dislocation structures needed to efficiently produce forest dislocations needed for strain hardening. As the indentation strain increases, the contact radius gradually increases and the strain hardening rate

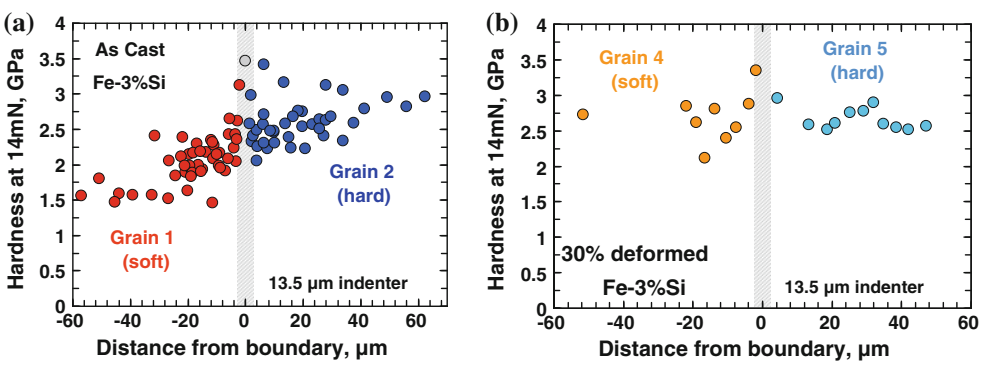

Fig. 5 Hardness profiles, calculated as the contact stress at 14 mN load for the 13.5 μm indenter, across **a** Grains 1 and 2 for the as-cast Fe–3%Si sample and **b** Grains 4 and 5 for the 30% deformed Fe–3%Si sample

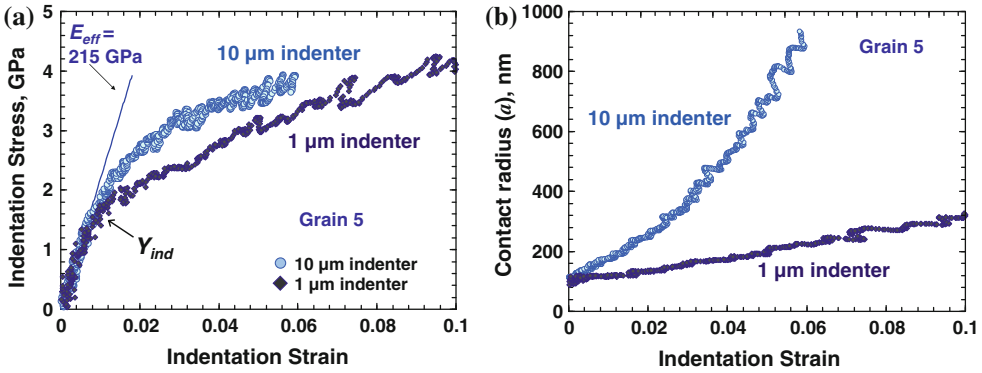

Fig. 6 Effect of indenter size on the indentation stress–strain curves from deformed samples. **a** While the indentation stress–strain curves obtained using two different indenter radii show a similar Y_{ind} value, the bigger 10 μm indenter shows larger strain hardening than the smaller 1 μm indenter. **b** Changes in contact radius a with indentation strain for the two different indenter sizes

appears to pick up. On the other hand, the contact radius increases much faster for the larger indenter. This appears to correspond well with the increased strain hardening rates obtained with the larger indenter.

Conclusions

In summary, we have demonstrated a novel way of characterizing the mechanical behavior of grain boundary regions in polycrystalline materials using spherical nanoindentation. This has been made possible by the combined use of OIM and our data analysis procedures for spherical nanoindentation which allow us to analyze the initial loading portion of the indentation stress–strain response. In this study, our analysis techniques have been able to characterize the indentation yield strengths of near grain boundaries regions in both as-cast and deformed samples, and estimate the percentage increases in local slip resistances. Analysis of the pop-in behavior across grain boundaries was also found to be a useful indicator of the boundary's potency as a dislocation source. Use of these new protocols over a larger number of different kinds of boundaries is expected to be very useful for correlating the structures of the grain boundaries with their mechanical response.

Acknowledgements Authors acknowledge funding from ARO grant W911NF-10-1-0409, Dr. Dejan Stojakovic's help in sample preparation, and many insightful discussions with Prof. Roger Doherty (Drexel University) in preparation of this manuscript. The authors thank Dr. Manuel Pouchon for allowing the use of the Agilent G200® nanoindentation system located at the Paul Scherrer Institut, Villigen, Switzerland, while the MTS XP® System used in this study is maintained and operated by the Centralized Research Facilities in the College of Engineering at Drexel University.

References

1. Hall EO (1951) Proc Phys Soc 64:747
2. Petch NJ (1953) Iron Steel Inst J 174:25
3. Lasalmonie A, Strudel JL (1986) J Mater Sci 21:1837. doi: 10.1007/BF00547918
4. Meyers M, Chawla K (2007) In: Mechanical Behavior Of Materials, Prentice-Hall, Upper Saddle River
5. Meyers MA, Ashworth E (1982) Philos Mag A 46:737
6. Li JCM (1963) Trans Metall Soc AIME 227:239
7. Bucaille JL, Stauss S, Felder E, Michler J (2003) Acta Mater 51: 1663
8. Stauss S, Schwaller P, Bucaille JL, Rabe R, Rohr L, Michler J, Blank E (2003) Microelectron Eng 67–68:818
9. Kalidindi SR, Pathak S (2008) Acta Mater 56:3523
10. Pathak S, Kalidindi SR, Klemenz C, Orlovskaya N (2008) J Eur Ceramic Soc 28:2213
11. Pathak S, Shaffer J, Kalidindi SR (2009) Scr Mater 60:439
12. Pathak S, Stojakovic D, Kalidindi SR (2009) Acta Mater 57:3020
13. Kunz A, Pathak S, Greer JR (2011) Acta Mater 59:4416
14. Ohmura T, Tsuzaki K, Fuxing Y (2005) Mater Trans 46:2026
15. Wang MG, Ngan AHW (2004) J Mater Res 19:2478
16. Lee CS, Han GW, Smallman RE, Feng D, Lai JKL (1999) Acta Mater 47:1823
17. Wo PC, Ngan AHW (2004) J Mater Res 19:189
18. Soifer YM, Verdyan A, Kazakevich M, Rabkin E (2002) Scr Mater 47:799
19. Ohmura T, Tsuzaki K (2008) J Phys D 41:074015
20. Goken M, Kempf M, Bordenet M, Vehoff H (1999) Surface Interface Anal 27:302
21. Ohmura T, Tsuzaki K (2007) J Mater Sci 42:1728. doi: 10.1007/s10853-006-0885-y
22. Soer WA, Aifantis KE, De Hosson JTM (2005) Acta Mater 53:4665
23. Soer WA, De Hosson JTM (2005) Mater Lett 59:3192
24. Eliash T, Kazakevich M, Semenov VN, Rabkin E (2008) Acta Mater 56:5640
25. Adams BL (1997) Ultramicroscopy 67:11
26. Adams BL, Wright SI, Kunze K (1993) Metall Trans A 24A:819
27. Pathak S, Stojakovic D, Doherty R, Kalidindi SR (2009) J Mater Res 24:1142
28. Britton TB, Randman D, Wilkinson AJ (2009) J Mater Res 24:607
29. Hertz H (1896) Miscellaneous Papers. MacMillan and Co. Ltd., New York
30. Johnson KL (1987) Contact Mechanics: Cambridge University Press, Cambridge
31. Sneddon IN (1965) Int J Eng Sci 3:47
32. Kalidindi SR, Bhattacharyya A, Doherty RD (2004) In: Proceedings of the Royal Society of London, Series A (Mathematical, Physical and Engineering Sciences) 460: 1935
33. Sun S, Adams BL, King WE (2000) Philos Mag A 80:9
34. Sun S, Adams BL, Shet C, Saigal S, King W (1998) Scr Mater 39:501
35. Zaefferer S, Kuo JC, Zhao Z, Winning M, Raabe D (2003) On the influence of the grain boundary misorientation on the plastic deformation of aluminum bicrystals. Acta Mater 51:4719